Field-Free Spin-Orbit-Torque Switching in Co/Pt/Co Multilayer with Mixed Magnetic Anisotropies

Stanisław Łazarski,[1,*] Witold Skowroński,[1] Jarosław Kanak,[1] Łukasz Karwacki,[1,2] Sławomir Ziętek,[1] Krzysztof Grochot,[1,3] Tomasz Stobiecki,[1,3] and Feliks Stobiecki[2]

[1]*Department of Electronics, AGH University of Science and Technology, Al. Mickiewicza 30, 30-059 Kraków, Poland*

[2]*Institute of Molecular Physics, Polish Academy of Sciences, ul. Smoluchowskiego 17, 60-179 Poznań, Poland*

[3]*Faculty of Physics and Applied Computer Science, AGH University of Science and Technology, Al. Mickiewicza 30, 30-059 Kraków, Poland*

Spin-orbit-torque- (SOT) induced magnetization switching in a Co/Pt/Co trilayer, with two Co layers exhibiting magnetization easy axes orthogonal to each other is investigated. A Pt layer is used as a source of spin-polarized current as it is characterized by relatively high spin-orbit coupling. The spin Hall angle of Pt, $\theta = 0.08$, is quantitatively determined using the spin-orbit-torque ferromagnetic resonance technique. In addition, Pt serves as a spacer between two Co layers and depending on its thickness, different interlayer-exchange-coupling (IEC) energy between ferromagnets is induced. Intermediate IEC energies, resulting in a top Co magnetization tilted from the perpendicular direction, allows for SOT-induced field-free switching of the top Co layer. The switching process is discussed in more detail, showing the potential of the system for neuromorphic applications.

I. INTRODUCTION

Manipulation of the magnetization of micro and nanostructures by electrical means allows for the design of low-energy and scalable spintronic devices [1]. A number of applications taking advantage of magnetic tunnel junctions (MTJs) and spin-valve structures, which utilize magnetoresistance and spin-transfer-torque (STT) [2,3] effects for operation, have been proposed. Magnetic tunnel junctions with an in-plane magnetic easy axis based on MgO have been among the most studied devices due to a high tunneling magnetoresistance (TMR) ratio [4], and current-induced magnetization switching [5] observed in the absence of an external magnetic field. Unfortunately, in general, they require high critical-current densities for the magnetization switching. Recently, MTJs with a perpendicular easy axis have been proposed to reduce this switching current and to enhance thermal stability of the free layer [6–8]. Nonetheless, the current densities used for switching may degrade MgO tunnel barrier properties with time, which hampers potential endurance of the device. On the other hand, spin-orbit-torque- (SOT) driven switching of magnetization with perpendicular magnetic anisotropy (PMA) has emerged and gained a lot of attention as it does not require high-density current flow via a thin MgO tunnel

barrier. Initially, SOT switching of perpendicularly magnetized ferromagnets has relied on an external magnetic field to break the time-reversal symmetry [9–11]. However, it would be impractical to use the external field for device application. By using antiferromagnets, the symmetry can be broken and magnetization switching in the absence of the external magnetic field can be achieved [12–17].

In this work, we present another concept utilizing two Co layers with orthogonal easy axes [18,19] that are coupled via interlayer exchange coupling (IEC) across a Pt spacer as for example in Ref. [20] to achieve SOT switching without the external magnetic field [21,22]. The magnetization of the top Co layer is tilted from the perpendicular direction due to ferromagnetic coupling with an in-plane magnetized bottom Co layer. In addition, the Pt spacer serves as a source of the spin current due to spin-orbit coupling characterized by the moderate spin Hall angle (θ_{SHE}) [10,23,24]. Moreover, the nonorthogonal direction of Co-layer magnetizations results in analogue-like switching behavior. This property of the device is potentially useful as a building block of a neuromorphic network utilizing spintronic elements [15].

II. EXPERIMENT

The following multilayer structure is investigated: Si/ SiO$_2$/Ti(2)/Co(3)/Pt(t_{Pt})/Co(1)/MgO(2)/Ti(2) (thickness in nm) with t_{Pt} varying from 0 to 4 nm. The

*lazarski@agh.edu.pl

thicker Co layer exhibits in-plane anisotropy, whereas the thinner one is characterized by effective perpendicular anisotropy. In order to determine the resistivity and SOT dynamics of Pt and Co, additional multilayer structures of Si/SiO$_2$/Co(5)/Pt(0-10) and Si/SiO$_2$/Ti(2)/Co(0-10)/Pt(4) are prepared. All samples are deposited using a magnetron sputtering system in an Ar atmosphere. After the deposition process, all samples are characterized by x-ray diffraction (XRD). X-ray reflectivity (XRR) measurements are made in order to control the thickness of particular layers in the system [25]. The texture is inspected using rocking-curve and polar-figure methods (see the Supplemental Material [26]). The Hall bars and stripes dedicated for spin-orbit-torque ferromagnetic resonance (SOT FMR) measurements are fabricated using electron-beam lithography, ion-beam etching, and a lift-off process. The nominal dimensions of samples are $w \times l$, where $w = 10, 20, 30$ μm and $l = 100$ μm for SOT-induced dynamics measurements and Hall bars of $w = 10, 20, 30$ μm and $l = 24$ μm for current-induced magnetization-switching experiments, Fig. 1. Electrical connections are fabricated using Al(20)/Au(30) contact pads of 100×100 μm. A dedicated multiprobe system, which enables sample rotation in a given plane under the external magnetic field, is used.

The resistivities of Co and Pt layers are determined in a Pt and Co wedge sample, as described in Ref. [27]. The Pt resistivity is almost constant $\rho_{Pt} \approx 23$ $\mu\Omega$cm, whereas the Co resistivity, ρ_{Co}, varied from 15 to 29 $\mu\Omega$cm with decreasing thickness. Detailed information is presented within the Supplemental Material [26]. We note that ρ_{Pt} is smaller than in our previous work [28] because in this case Pt is deposited on high-textured Co, in contrast to Pt deposited on amorphous Co-Fe-B. The SOT FMR measurements are conducted in an in-plane magnetic field applied at an 45° angle with respect to the long stripe axis and rf-signal power of 16 dBm. The dc voltage

originating from the mixing between oscillating resistance (due to SOT and magnetoresistance) and in-phase charge current are measured using a lock-in amplifier, which is synchronized with an amplitude modulated rf source. The SOT-induced switching experiment is performed in both in-plane and perpendicular magnetic fields. In order to show the analoguelike behavior, the experiment with varying time of the switching pulses between 500 μs and 500 ms is performed.

III. RESULTS AND DISCUSSION

Spin-transport properties of Pt, such as the spin Hall angle and spin-diffusion length, are determined using a dedicated model based on Ref. [28]. Mixing voltage, V_{mix}, is obtained from the SOT FMR measurement as a function of magnetic field, H, and the results are presented in Fig. 2. The signal consists of two parts (symmetric and antisymmetric), which are modeled using Lorentz curves,

$$V_{mix} = V_S \frac{\Delta H^2}{\Delta H^2 + (H - H_0)^2} + V_A \frac{\Delta H(H - H_0)}{\Delta H^2 + (H - H_0)^2},$$
(1)

where V_S (V_A) is the magnitude of symmetrical (antisymmetrical) Lorentz curve, ΔH is the linewidth, and H_0 is the resonance field.

We assume that the greatest contribution to magnetoresistance comes from the spin Hall magnetoresistance (SMR) effect, which can be described in this case via the model developed in Ref. [29],

$$\frac{\Delta R}{R_{Pt}} \approx \frac{\theta^2 \lambda}{t_{Pt}} \left[\frac{g_{Pt}^R}{1 + g_{Pt}^R} - \frac{g_{Pt}^{Co}}{1 + g_{Pt}^{Co} \coth(t_{Pt}/\lambda)} \right]$$
$$\times \tanh \frac{t_{Pt}}{\lambda} \tanh^2 \frac{t_{Pt}}{2\lambda},$$
(2)

where $R_{Pt} = l\rho_{Pt}/(t_{Pt}w)$, and λ is the resistance, the spin Hall angle, and the spin-diffusion length of Pt. Respectively, $g_{Pt}^R = 2e^2/\hbar\lambda\rho_{Pt}G^R \coth(t_{Pt}/\lambda)$ is the real part of
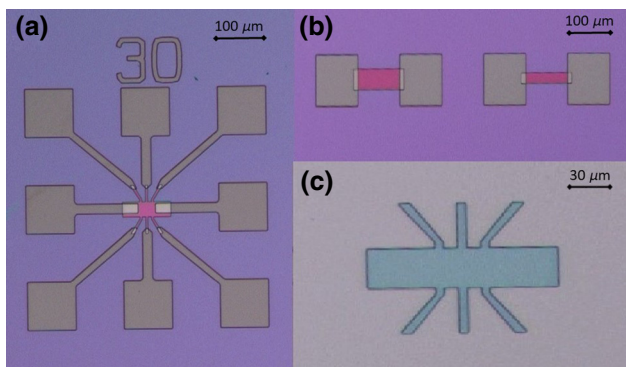

FIG. 1. Layout of the fabricated devices used for different measurements: (a) Hall bar for SOT-induced switching, (b) stripes of different width for SOT dynamics. Detailed dimensions of the Hall bar are given in (c).
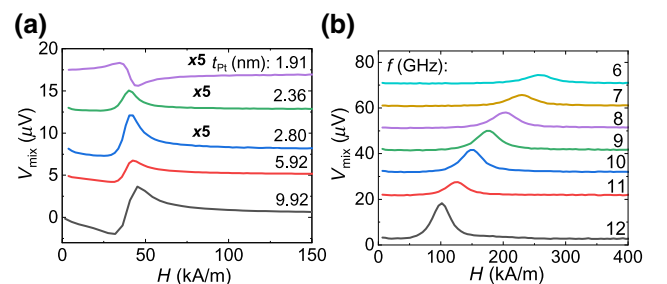

FIG. 2. V_{mix} as a function of magnetic field measured in bilayers for different Pt thicknesses with excitation frequency $f = 4$ GHz (a) and fixed $t_{Pt} = 2.36$ nm with different f (b). Curves are artificially offset for clarity.

dimensionless spin-mixing conductance with G^R being the real part of spin-mixing conductance, and

$$g_{\mathrm{Pt}}^{\mathrm{Co}} = \frac{(1-p^2)\rho_{\mathrm{Pt}}\lambda}{\rho_{\mathrm{Co}}\lambda_{\mathrm{Co}}\coth(t_{\mathrm{Co}}/\lambda_{\mathrm{Co}})} \qquad (3)$$

is the dimensionless spin conductivity of the Pt/Co interface, where p is the spin polarization of Co at the Fermi level, and λ_{Co} is the spin-diffusion length in the Co layer [29].

The symmetric component to the signal is known to originate from the spin Hall effect induced antidampinglike field [28],

$$H_{\mathrm{DL}} \approx -\frac{\hbar j_c^{\mathrm{Pt}}}{2eM_s t_{\mathrm{Co}}}\theta\left[1 - \mathrm{sech}\frac{t_{\mathrm{Pt}}}{\lambda}\right]\frac{g_{\mathrm{Pt}}^R}{1+g_{\mathrm{Pt}}^R}, \qquad (4)$$

where M_s is the saturation magnetization of Co, and j_c^{Pt} is the current density in the Pt layer. Moreover, in the derivation of formula (3) we assume a negligible imaginary part of spin-mixing conductance. The antisymmetric component, on the other hand, is dominated by contributions from the Oersted field,

$$H_{\mathrm{Oe}} = -\frac{j_c^{\mathrm{Pt}} t_{\mathrm{Pt}}}{2}, \qquad (5)$$

and interfacial Rashba-Edelstein contribution,

$$H_{\mathrm{SO}} = \Gamma_{\mathrm{SO}}, \qquad (6)$$

which is determined by thickness-independent spin-orbit coupling strength Γ_{SO} [28]. We consider here this contribution as originating from interfacial spin-orbit coupling, and distinct from spin Hall contribution, as predicted theoretically [30], although it is still the subject of an ongoing debate. Experimental works, however, seem to confirm the possible Rashba-Edelstein origin of the field [31,32]. Note that an interfacial contribution might be also attributed to the magnetic proximity effect from a ferromagnet [33,34], which was recently discussed by Zhu *et al.* [35]. The authors showed that the proximity effect in Co/Pt and $\mathrm{Au}_{25}\mathrm{Pt}_{75}$/Co interfaces has minimal correlation on either dampinglike or fieldlike spin-orbit torques compared to other interfacial effects like interfacial spin-orbit scattering. The relevant parameters used to model the effective fields are summarized in Table I.

The components V_S and V_A, obtained from Lorentz curve modeling for Co/Pt bilayers, are presented in Figs. 3(a) and 3(c) as functions of t_{Pt}. These dependencies are further fitted with Eqs. (4)–(6). As a result, the spin Hall angle of $\theta = 0.08$ is obtained, which agrees with literature values for this material [28,36]. Note, that in Fig. 3(d) the effective spin Hall angle, $\theta^{\mathrm{eff}} \approx 0.1$, obtained roughly from ratio V_S/V_A is slightly larger than the spin Hall angle

TABLE I. Magnetotransport parameters of the modeled Co/Pt bilayer system.

Model	Value	Fitted	Value
λ_{Co}	1 nm[a]	θ	0.08
p	0.75[a]	λ	2.17 nm
$G^R/(e^2/\hbar)$	$3.9 \times 10^{19}\ \Omega^{-1}\,\mathrm{cm}^{-2}$	Γ_{SO}	119 A/m

[a]Ref. [29].

of Pt, $\theta = 0.08$, obtained from fitting the model derived in Ref. [28] to the data. As shown there, the spin Hall angle is treated as a bulk property of heavy metal layer and agrees with the effective spin Hall angle for thick Pt.

Next, we focus on multilayer structures with two Co layers (3 and 1 nm) separated by a Pt spacer of different thickness. Thicker (thinner) Co is characterized by in-plane (perpendicular) magnetic anisotropy, which is manifested by the shape of the anomalous Hall effect (AHE) hysteresis loop [Fig. 4(a)]. In addition, these two layers are ferromagnetically coupled, and the energy of this coupling varies with t_{Pt} [20]. To quantitatively determine the coupling energy, AHE curves for different Pt spacers are modeled using a macrospin approach [37], and the energy values are depicted in Fig. 4(c). For high coupling energies (corresponding to $t_{\mathrm{Pt}} < 3$ nm) the AHE loop is hysteresis-free. For the spacer thickness of $t_{\mathrm{Pt}} > 3$ nm, hysteresis in AHE is observed, which enables the SOT-induced switching presented below.

As shown above, the top Co layer is tilted from the perpendicular direction due to ferromagnetic coupling with
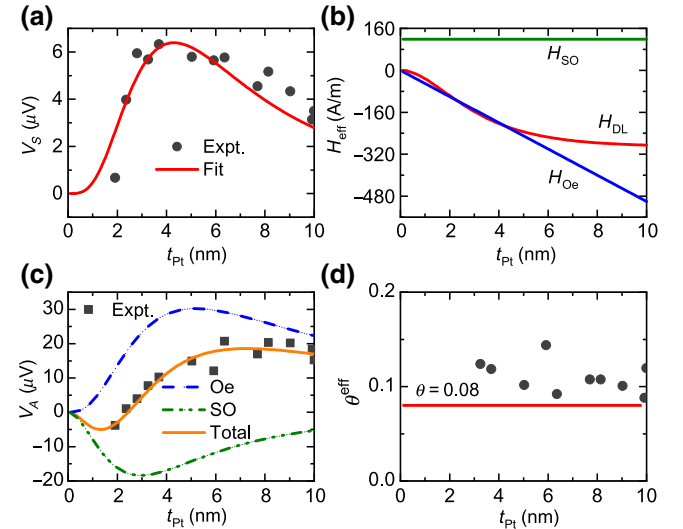

FIG. 3. Experimental and fitted amplitudes, from Eqs. (4)–(6), of symmetric, V_S, and antisymmetric, V_A, components to the signal, V_{mix}, are shown as functions of thickness t_{Pt} in (a) and (c), respectively. The contribution of each effective field is shown in (b). Effective spin Hall angle and spin Hall angle of Pt obtained from fitting Eq. (4) to the data are shown in (d).
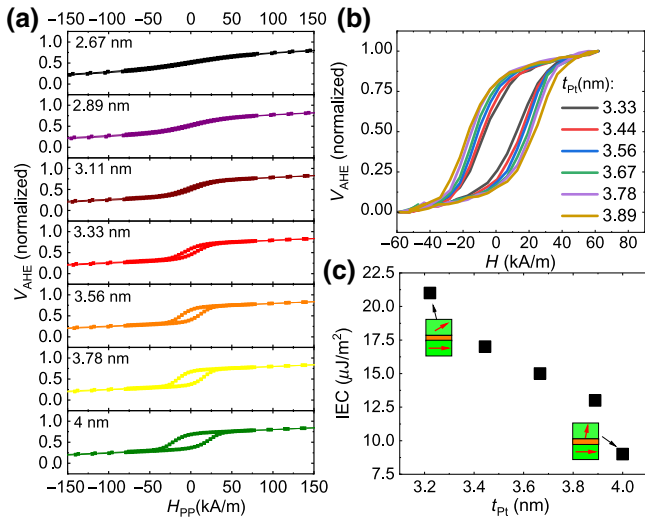
FIG. 4. AHE hysteresis loops measured in trilayers with different Pt spacer thicknesses (a). Open hysterisis loops are measured for $t_{Pt} > 3$ nm (b). IEC energy as a function of t_{Pt} is depicted in (c). The image presents effective magnetization direction in the top and bottom Co layers.

FIG. 5. SOT-induced switching process under different external magnetic fields for a trilayer with a spacer thickness of $t_{Pt} = 3.68$ nm. Hall voltage hysteresis loops as a function of in-plane current measured under various in-plane magnetic fields changed from negative to positive (a) and positive to negative (b) values. Corresponding critical currents for different fields are presented in (c),(d).

a bottom in-plane magnetized Co layer. Such symmetry breaking is essential for a field-free SOT-induced magnetization switching. Figures 5(a) and 5(b) present the magnetization state of the top Co (described with AHE voltage) as a function of an in-plane current (I) for different in-plane magnetic fields, when the magnetic field is increased (a) and decreased (b). The measurement protocol is the following: first, the sample is magnetized in a saturating negative magnetic field. Next, the field is set to -160 kA/m and the current is swept from 0 to -100 mA, then to positive 100 mA and back to 0 mA. Counterclockwise V_{AHE} versus I loops are measured with magnetic fields up to around 12 kA/m. Greater field values result in clockwise V_{AHE} versus I loops. Afterwards, the sample is magnetized in positive saturating magnetic field and V_{AHE} versus I loops are measured at H starting from 160 kA/m to -160 kA/m. In contrast to the previous case, clockwise loops change to counterclockwise at $H = -12$ kA/m. The switching current depends linearly on the magnetic field value according to Ref. [38]. The change in transition from 12 kA/m to -12 kA/m originates from the in-plane magnetized bottom Co switching, and is different than in the case of heterostructures using antiferromagnets [15].

The critical currents and current densities for several Pt thicknesses are summarized in Table II. As expected, the critical current needed to switch top Co magnetization without the external magnetic field decreases with increasing IEC energy.

Finally, we move on to the description of the analog SOT switching of a thin Co layer. As seen in SOT-switching experiments, AHE voltage changes
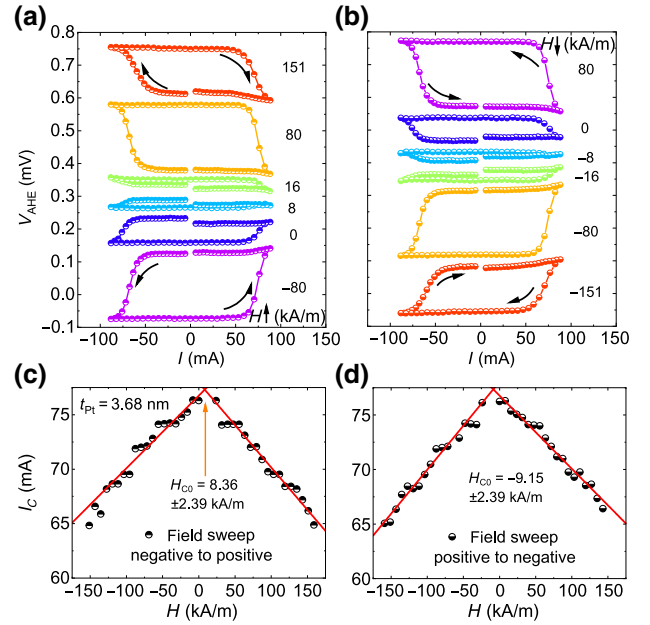
gradually with the current, in contrast to the current-induced switching required typically for digital memory applications [11]. Figure 6(a) presents Hall resistance $R_H = V_{AHE}/I$ of a trilayer with a Pt spacer thickness of $t_{Pt} = 3.2$ nm.

After initialization in a saturating perpendicular magnetic field, R_H changes from a minimal value of $R_{H\text{-min}} = -0.14$ Ω to around 0.07 Ω upon negative current application. Note that maximal resistance for this spacer thickness is $R_{H\text{-max}} = 0.14$ Ω, so no saturation is achieved during SOT switching. Sweeping the current from negative to positive values induces switching to a lower R_H; however, only down to around $R_H = -0.07$ Ω, which is above $R_{H\text{-min}}$. Therefore, during SOT-induced switching, the magnetization state is not reversed fully, but possibly

TABLE II. Summary of critical switching currents, I_{c0}, and current densities, J_{c0}, of Co/Pt/Co trilayers for different Pt thickness, t_{Pt}.

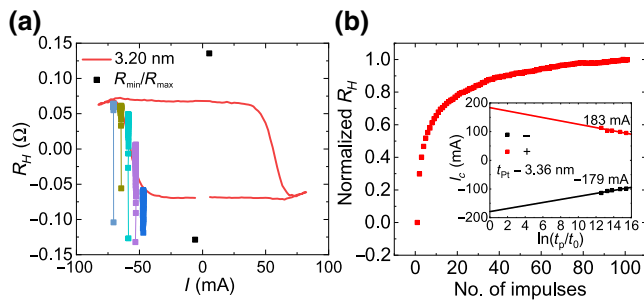| t_{Pt} (nm)	I_{c0} (mA)	J_{c0} (A/m^2)
3.7	77	$7.00 \cdot 10^{11}$
3.6	70	$6.50 \cdot 10^{11}$
3.4	61	$6.02 \cdot 10^{11}$
2.9	51	$5.95 \cdot 10^{11}$

FIG. 6. Hall resistance loops as a function of current for $t_{Pt} = 3.2$ nm. Full black squares in (a) corresponds to the initial resistance after saturation in a magnetic field. Squares of different colors indicate the resistance state after application of up to a hundred current pulses of given amplitude. Normalized resistance after a different number of pulses of around 60-mA amplitude is presented in (b). Both (a),(b) highlight the neuromorphiclike behavior of the sample. Inset: the switching-current density dependence on the switching-pulse duration (t_p). t_0 is the inverse of the attempt frequency equal to 1 ns.

a magnetization domain state is formed. A detailed discussion on the switching mechanism in a similar stack is presented in Refs. [39] and [40]. Moreover, R_H depends also on the number of pulses of the same amplitude, as well as the pulse duration, Fig. 6(b). By decreasing the switching-pulse duration time (t_p) from 500 ms down to 500 μs, the absolute value of the critical current increases according to Ref. [41]. Nonetheless, such a gradual change in Hall resistivity mimics the behavior of a neuron, whose resistive potential changes based on electrical signals delivered by synapses in an analog manner [42].

IV. SUMMARY

In summary, SOT-induced switching in the Co/Pt/Co structure with in-plane and perpendicular anisotropy of Co layers coupled ferromagnetically by the Pt spacer with varying thickness is investigated. The spin Hall angle and spin-diffusion length are determined using the SOT FMR method, the results of which are analyzed using the dedicated theoretical model. The coupling between two Co layers is tuned by the Pt spacer thickness and for intermediate thickness, 2.9 nm $< t_{Pt} <$ 3.7 nm, field-free SOT-induced switching of the perpendicularly magnetized Co layer is observed. For a range of the Pt spacer thicknesses, gradual magnetization change with in-plane current is obtained, which may be useful for the hardware implementation of a spintronic neuromorphic network.

ACKNOWLEDGMENTS

[1] S. Bhatti, R. Sbiaa, A. Hirohata, H. Ohno, Sh. Fukami, and S. N. Piramanayagam, Spintronics based random access-memory: A review, Mater. Today **20**, 530 (2017).

[2] J. C. Slonczewski, Current-driven excitation of magnetic multilayers, J. Magn. Magn. Mater. **159**, L1 (1996).

[3] L. Berger, Emission of spin waves by a magnetic multilayer traversed by a current, Phys. Rev. B **54**, 9353 (1996).

[4] S. Ikeda, J. Hayakawa, Y. Ashizawa, Y. M. Lee, K. Miura, H. Hasegawa, M. Tsunoda, F. Matsukura, and H. Ohno, Tunnel magnetoresistance of 604% at 300 K by suppression of Ta diffusion in CoFeB/MgO/CoFeB pseudo-spin-valves annealed at high temperature, Appl. Phys. Lett. **93**, 082508 (2008).

[5] Y. Huai, F. Albert, P. Nguyen, M. Pakala, and T. Valet, Observation of spin-transfer switching in deep submicron-sized and low-resistance magnetic tunnel junctions, Appl. Phys. Lett. **84**, 3118 (2004).

[6] S. Ikeda, K. Miura, H. Yamamoto, K. Mizunuma, H. D. Gan, M. Endo, S. Kanai, J. Hayakawa, F. Matsukura, and H. Ohno, A perpendicular-anisotropy CoFeB-MgO magnetic tunnel junction, Nat. Mater. **9**, 721 (2010).

[7] M. Nakayama, T. Kai, N. Shimomura, M. Amano, E. Kitagawa, T. Nagase, M. Yoshikawa, T. Kishi, S. Ikegawa, and H. Yoda, Spin transfer switching in TbCoFe/CoFeB/MgO/CoFeB/TbCoFe magnetic tunnel junctions with perpendicular magnetic anisotropy, J. Appl. Phys. **103**, 07A710 (2008).

[8] P. K. Amiri, Z. M. Zeng, J. Langer, H. Zhao, G. Rowlands, Y.-J. Chen, I. N. Krivorotov, J.-P. Wang, H. W. Jiang, J. A. Katine, Y. Huai, K. Galatsis, and K. L. Wang, Switching current reduction using perpendicular anisotropy in CoFeB-MgO magnetic tunnel junctions, Appl. Phys. Lett. **98**, 112507 (2011).

[9] I. M. Miron, K. Garello, G. Gaudin, P.-J. Zermatten, M. V. Costache, S. Auffret, S. Bandiera, B. Rodmacq, A. Schuhl, and P. Gambardella, Perpendicular switching of a single ferromagnetic layer induced by in-plane current injection, Nature **476**, 189 (2011).

[10] L. Liu, O. J. Lee, T. J. Gudmundsen, D. C. Ralph, and R. A. Buhrman, Current-Induced Switching of Perpendicularly Magnetized Magnetic Layers Using Spin Torque from the Spin Hall Effect, Phys. Rev. Lett. **109**, 096602 (2012).

[11] L. Liu, C.-F. Pai, Y. Li, H. W. Tseng, D. C. Ralph, and R. A. Buhrman, Spin-torque switching with the giant Spin hall effect of tantalum, Science **336**, 555 (2012).

[12] J. B. S. Mendes, R. O. Cunha, O. A. Santos, P. R. T. Ribeiro, F. L. A. Machado, R. L. Rodrîguez-Suárez, A. Azevedo, and S. M. Rezende, Large inverse spin Hall effect in the antiferromagnetic metal Ir$_{20}$Mn$_{80}$, Phys. Rev. B **89**, 140406(R) (2014).

[13] Y. Ou, S. Shi, D. C. Ralph, and R. A. Buhrman, Strong spin Hall effect in the antiferromagnet PtMn, Phys. Rev. B **93,** 220405(R) (2016).

[14] Y.-W. Oh, S.-H. Ch. Baek, Y. M. Kim, H. Y. Lee, K.-D. Lee, Ch.-G. Yang, E.-S. Park, K.-S. Lee, K.-W. Kim, G. Go, J.-R. Jeong, B.-Ch. Mim, H.-W. Lee, K.-J. Lee, and B.-G. Park, Field-free switching of perpendicular magnetization through spin-orbit torque in antiferromagnet/ferromagnet/oxide structures, Nat. Nanotechnol. **11,** 878-884 (2016).

[15] S. Fukami, C. Zhang, S. DuttaGupta, A. Kurenkov, and H. Ohno, Magnetization switching by spin-orbit torque in an antiferromagnet-ferromagnet bilayer system, Nat. Mater. **15,** 535 (2016).

[16] D. Wu, G. Yu, C.-T. Chen, S. A. Razavi, Q. Shao, X. Li, B. Zhao, K. L. Wong, C. He, Z. Zhang, P. K. Amiri, and K. L. Wang, Spin-orbit torques in perpendicularly magnetized $Ir_{22}Mn_{78}/Co_{20}Fe_{60}B_{20}/MgO$ multilayer, Appl. Phys. Lett. **109,** 222401 (2016).

[17] S. A. Razavi, D. Wu, G. Yu, Y.-C. Lau, K. L. Wong, W. Zhu, C. He, Z. Zhang, J. M. D. Coey, P. Stamenov, P. K. Amiri, and K. L. Wang, Joule Heating Effect on Field-Free Magnetization Switching by Spin-Orbit Torque in Exchange-Biased Systems, Phys. Rev. Appl. **7,** 024023 (2017).

[18] P. Baláž, M. Gmitra, and J. Barnaś, Current-induced dynamics in noncollinear dual spin valves, Phys. Rev. B **80,** 174404 (2009).

[19] Y.-Ch. Lau, D. Betto, K. Rode, J. M. D. Coey, and P. Stamenov, Spin-orbit torque switching without an external field using interlayer exchange coupling, Nat. Nanotechnol. **11,** 758-762 (2016).

[20] M. Matczak, R. Schafer, M. Urbaniak, B. Szymański, P. Kuświk, A. Jarosz, M. Schmidt, J. Aleksiejew, S. Jurga, and F. Stobiecki, Domain wall generated by graded interlayer coupling in Co/Pt/Co film with perpendicular anisotropy, Appl. Phys. Lett. **107,** 012404 (2015).

[21] G. Yu, P. Upadhyaya, Y. Fan, J. G. Alzate, W. Jiang, K. L. Wong, S. Takei, S. A. Bender, L.-T. Chang, Y. Jiang, M. Lang, J. Tang, Y. Wang, Y. Tserkovnyak, P. K. Amiri, and K. L. Wang, Switching of perpendicular magnetization by spin-orbit torques in the absence of external magnetic fields, Nat. Nanotechnol. **9,** 548 (2014).

[22] L. You, O.-J. Lee, D. Bhowmik, D. Labanowski, J. Hong, J. Bokor, and S. Salahuddin, Switching of perpendicularly polarized nanomagnets with spin orbit torque without an external magnetic field by engineering a tilted anisotropy, Proc. Natl. Acad. Sci. U. S. A. **112,** 10310 (2015).

[23] S. Emori, U. Bauer, S. M. Ahn, E. Martinez, and G. S. D. Beach, Current-driven dynamics of chiral ferromagnetic domain walls, Nat. Mater. **12,** 611 (2013).

[24] S. Woo, M. Mann, A. J. Tan, L. Garetta, and G. S. D. Beach, Enhanced spin-orbit torques in Pt/Co/Ta heterostructures, Appl. Phys. Lett. **105,** 212404 (2014).

[25] J. Kanak, P. Wiśniowski, T. Stobiecki, A. Zaleski, W. Powroźnik, S. Cardoso, and P. P. Freitas, X-ray diffraction analysis and Monte Carlo simulations of CoFeB-MgO based magnetic tunnel junctions, J. Appl. Phys. **113,** 023915 (2013).

[26] See Supplemental Material at http://link.aps.org/supplemental/10.1103/PhysRevApplied.12.014006 for a detailed description of the structural characterization, the resistivity analysis and magnetisation saturation measurements.

[27] M. Kawaguchi, D. Towa, Y.-C. Lau, S. Takahashi, and M. Hayashi, Anomalous spin Hall magnetoresistance in Pt/Co bilayers, Appl. Phys. Lett. **112,** 202405 (2018).

[28] W. Skowroński, Ł. Karwacki, S. Ziętek, J. Kanak, S. Łazarski, K. Grochot, T. Stobiecki, P. Kuświk, F. Stobiecki, and J. Barnaś, Determination of Spin Hall Angle in Heavy-Metal/Co-Fe-B-Based Heterostructures with Interfacial Spin-Orbit Fields, Phys. Rev. Appl. **11,** 024039 (2019).

[29] J. Kim, P. Sheng, S. Takahashi, S. Mitani, and M. Hayashi, Spin Hall Magnetoresistance in Metallic Bilayers, Phys. Rev. Lett. **116,** 097201 (2016).

[30] P. M. Haney, H.-W. Lee, K.-J. Lee, A. Manchon, and M. D. Stiles, Current induced torques and interfacial spin-orbit coupling: Semiclassical modeling, Phys. Rev. B **87,** 174411 (2013).

[31] A. Kawasuso, Y. Fukaya, M. Maekawa, H. Zhang, T. Seki, T. Yoshino, E. Saitoh, and K. Takanashi, Current-induced spin polarization on a Pt surface: A new approach using spin-polarized positron annihilation spectroscopy, J. Magn. Magn. Mater. **342,** 139 (2013).

[32] G. Allen, S. Manipatruni, D. E. Nikonov, M. Doczy, and I. A. Young, Experimental demonstration of the coexistence of spin Hall and Rashba effects in β-tantalum/ferromagnet bilayers, Phys. Rev. B **91,** 144412 (2015).

[33] T. Koyama, Y. Guan, Y. Hibino, M. Suzuki, and D. Chiba, Magnetization switching by spin-orbit torque in Pt with proximity-induced magnetic moment, J. Appl. Phys. **121,** 123903 (2017).

[34] T. A. Peterson, A. P. McFadden, C. J. Palmstrøm, and P. A. Crowell, Influence of the magnetic proximity effect on spin-orbit torque efficiencies in ferromagnet/platinum bilayers, Phys. Rev. B **97,** 020403(R) (2018).

[35] L. J. Zhu, D. C. Ralph, and R. A. Buhrman, Irrelevance of magnetic proximity effect to spin-orbit torques in heavy-metal/ferromagnet bilayers, Phys. Rev. B **98,** 134406 (2018).

[36] J. C. Rojas-Sánchez, N. Reyern, P. Laczkowski, W. Savero, J. P. Attané, C. Deranlot, M. Jamet, J. M. George, L. Vila, and H. Jaffrès, Spin Pumping and Inverse Spin Hall Effect in Platinum: The Essential Role of Spin-Memory Loss at Metallic Interfaces, Phys. Rev. Lett. **112,** 106602 (2014).

[37] M. Czapkiewicz, M. Żołądz, J. Wrona, P. Wiśniowski, R. Rak, T. Stobiecki, C. G. Kim, C. O. Kim, M. Takahashi, and M. Tsunoda, Magnetization process and domains in MTJ, Phys. Status Solidi **241,** 1477 (2004).

[38] K.-S. Lee, S.-W. Lee, B.-C. Min, and K.-J. Lee, Threshold current for switching of a perpendicular magnetic layer induced by spin Hall effect, Appl. Phys. Lett. **102,** 112410 (2013).

[39] M. Baumgartner, K. Garello, J. Mendil, C. O. Avci, E. Grimaldi, C. Murer, J. Feng, M. Gabureac, C. Stamm, Y. Acremann, S. Finizio, S. Wintz, J. Raabe, and P. Gambardella, Spatially and time-resolved magnetization

dynamics driven by spin-orbit torques, Nat. Nanotechnol. **12**, 980 (2017).

[40] M. M. Decker, M. S. Wörnle, A. Meisinger, M. Vogel, H. S. Körner, G. Y. Shi, C. Song, M. Kronseder, and C. H. Back, Time Resolved Measurements of the Switching Trajectory of Pt/Co Elements Induced by Spin-Orbit Torques, Phys. Rev. Lett. **118**, 257201 (2017).

[41] H. Kubota, A. Fukushima, Y. Ootani, S. Yuasa, and K. Ando, Dependence of spin-transfer switching current on free layer thickness in Co-Fe-B/MgO/Co-Fe-B magnetic tunnel junctions, Appl. Phys. Lett. **89**, 032505 (2006).

[42] P. Krzysteczko, G. Reiss, and A. Thomas, Memristive switching of MgO based magnetic tunnel junctions, Appl. Phys. Lett. **95**, 112508 (2009).